J Mater Sci: Mater Electron

Device-relevant properties of [010]-oriented undoped TGS single crystals grown above and below the phase transition temperature

Muthu Senthil Pandian[1,*], Sunil Verma[2,3], P. Karuppasamy[1], P. Ramasamy[1], V. S. Tiwari[2,3], and A. K. Karnal[2,3]

[1] SSN Research Centre, Sri Sivasubramaniya Nadar College of Engineering, Chennai 603110, Tamilnadu, India
[2] Laser & Functional Materials Division, Raja Ramanna Centre for Advanced Technology, Indore 452013, Madhya Pradesh, India
[3] Homi Bhabha National Institute, BARC Training School Complex, Anushakti Nagar, Mumbai 400094, Maharashtra, India

Received: 27 October 2020
Accepted: 4 May 2021

ABSTRACT

Undoped triglycine sulfate (TGS) crystals grown above and below its Curie temperature (T_c) along [010] polar direction by unidirectional solution growth method were characterized to measure and compare their device-relevant properties. The powder XRD was used for phase confirmation. The piezoelectric coefficient of TGS crystal grown below T_c was higher than that grown above T_c, and the P–E hysteresis studies show well-saturated hysteresis loops for both the crystals and the values of remnant polarization and coercive field were higher for crystal grown above T_c as compared to crystal grown below T_c. These observations were explained on the basis of the concentration of point defects and their influence on the domain nucleation and mobility. The crystal grown above T_c also exhibits higher dielectric permittivity, high mechanical hardness, low dislocations defects density, showing its improved device potential compared to TGS crystal grown below T_c. The probable reasons for the characterization results have been presented.

1 Introduction

The ferroelectric activity in triglycine sulfate (TGS) crystal was discovered by Matthias et al. in 1956 [1]. TGS crystals exhibit a second-order phase transition with an order–disorder character. The phase transition occurs at ~ 49 °C, with the appearance of a mirror plane in the paraelectric phase leading to the centrosymmetric monoclinic space group $P2_1/m$. In the ferroelectric phase, the mirror plane vanishes and the crystal exhibits the non-centrosymmetric monoclinic space group $P2_1$ [2]. TGS crystal is used for infrared (IR) detectors, sensors, and imaging applications due to its good ferroelectric behavior, the higher value of the pyroelectric and piezoelectric coefficient, and reasonably low dielectric constant [3]. The b-cut (010) face of TGS crystal, which is also the cleavage plane, is used for infrared detector

Address correspondence to E-mail: senthilpandianm@ssn.edu.in

https://doi.org/10.1007/s10854-021-06131-x
Published online: 16 May 2021

fabrication [4]. For VIDICON applications and laser energy meters, large area plates perpendicular to the polar axis are required. These are typically between 2.5 and 7.5 cm in diameter.

Many research groups have tried to tailor the physical properties of TGS crystal with amino acid dopants to meet the practical device fabrication requirements [5, 6]. To modify and improve the properties for applications, a wide range of inorganic and metallic dopants have been attempted in TGS crystal [7–9]. We have previously reported the unidirectional, bulk growth of pure and doped TGS crystals along [001] and [010] by the Sankaranarayanan–Ramasamy (SR) method, and their physical properties were studied [10–12]. The enhancement of crystalline properties in dye-doped TGS crystals is discussed by Sinha et al. [13]. TGS crystals were also grown below 0 °C, and their electro-physical properties were presented [14]. To investigate the influence of gravity on the defects structure of TGS crystal, it was also grown in the low gravity environment in space during the First International Microgravity Laboratory mission [15]. Investigations on the thermal diffusivity and thermal conductivity of pure and doped TGS crystals are reported by Ballard et al. [16] and Krajewski et al. [17]. Keve et al. [18] have studied the structural inhibition of ferroelectric switching in TGS. The critical phenomena associated with the ferroelectric phase transition in TGS crystals are investigated by several authors [19, 20]. Different authors have dealt with the characteristics of linear thermal expansion of a deuterated analog of TGS [21, 22]. The effect of hydrostatic pressure on the structural and electronic properties of TGS crystals is also investigated extensively [23]. Electron emission from ferroelectrics induced by the AC electric field in the vicinity of the phase transition is reviewed and discussed by Biedrzycki [24]. The effect of doping on the optical and communication properties of TGS has been discussed by Sinha et al. [25].

In the early years, several groups focused on the theoretical investigations on TGS material [16–24]; however, in the last two decades, several research groups have focused on the crystal growth of pure and doped TGS crystals for device purposes [5–15]. The researchers have developed various techniques such as the platform method, cylindrical seed technique, rotating disc technique, and reciprocating motion technique to get large size TGS crystals along the polar b-axis for detector fabrication [25, 26]. The efforts were mainly focused on improving the crystalline perfection and physical properties of the TGS crystals. The Sankaranarayanan-Ramasamy (SR) unidirectional solution growth method has proved its utility and advantages in the growth of several important crystals required for various device applications [27–30]. Recently, we have reported the use of this method to grow pure and doped TGS crystals along [010] polar direction in two temperature regimes, below and above its Curie temperature of 49 °C [10–12]. To the best of our knowledge, comparative investigations of the device-relevant physical properties of these crystals have not been reported before in the literature. In the present paper, detailed comparative investigations on the device-relevant physical properties of pure TGS crystals grown below and above T_c along [010] direction by SR unidirectional solution growth method are presented.

1.1 [010]-oriented growth of undoped TGS crystal above and below T_c

The results of chemical synthesis, bulk crystal growth, apparatus design and development, growth kinetics, and analysis of the morphology of pure TGS crystals in temperature ranges above and below its Curie temperature, by conventional slow cooling as well as unidirectional Sankaranarayana–Ramasamy method along [010] polar direction are reported elsewhere by the authors [11]. Therefore, only a summary of the growth results is presented here, and the main aim of the present paper is comparative investigations of the device-relevant physical properties.

1.2 Unidirectional growth below T_c

Approximately 600 ml of TGS solution saturated at 32 °C (solubility of 36 g/100 ml) was prepared. The solution in the top portion of the ampoule was maintained at 36 °C, whereas the solution in the bottom region near to the seed crystal was maintained at 26 °C. The experimental apparatus for the growth of undoped TGS below T_c is shown in Fig. 1a. After 40 days of continuous growth, a highly transparent undoped TGS crystal of length 60 mm and diameter 15 mm, oriented along [010] direction was

obtained, as shown in Fig. 1b. The cut and polished (010) element is shown in Fig. 1c.

1.3 Unidirectional growth above T_c

Approximately 700 ml of TGS solution saturated at 55 °C (solubility of 67 g/100 ml) was prepared. The optimized temperature of the solution in the top and bottom portion of the ampoule was 55 °C. The solution was cooled at 0.01 °C/h from 55 to 52.5 °C to grow the crystal. The experimental apparatus for the growth of TGS above T_c is shown in Fig. 2a. After 17 days of continuous growth, a highly transparent undoped TGS crystal of length 35 mm and diameter 15 mm, oriented along [010] direction was obtained, as shown in Fig. 2b. The cut and polished (010) element is shown in Fig. 2c.

2 Comparative characterization analysis

2.1 X-ray diffraction analysis of [010]-oriented undoped TGS crystals grown above and below T_c

Powder X-ray diffraction (PXRD) studies were carried out using Rigaku Geigerflex X-ray diffractometer employing CuKα (1.5405 Å) radiation. The scanning angle was varied from 10° to 70° with a scan speed of 2°/min. The diffraction patterns of crystals grown above and below T_c are shown in Fig. 3a, b. The PXRD data were used as the input for lattice parameter calculation using "POWDERX" software. It was confirmed that the grown single crystals belong to the monoclinic system and the cell parameters were a = 9.41Å, b = 12.64Å, c = 5.73Å with angle β = 110.35°, which match with the literature values [5]. The variation in the intensities of the XRD peaks of the two crystals and appearance of a few additional peak in the crystal grown above Tc may be attributed to the difference in the density of point defects in the two crystals. The observed prominent peaks of pure TGS are (001), (101), (11$\bar{1}$) (220), (121) (040), (211), and (231). The sharp peaks and low full-width at half maximum (FWHM) confirm the high crystalline perfection of the grown crystals.

2.2 Piezoelectric d_{33} coefficient

Thin plates were cleaved perpendicular to the [010] direction from the undoped TGS crystals grown below and above T_c for comparative analysis of d_{33} piezoelectric properties at room temperature using a piezometer system. The samples were subsequently lapped and polished. The samples were coated with gold in the argon atmosphere on either side to form electrodes using a sputtering unit (Emitech K 550X model). A precision force generator was used to apply a calibrated force of 0.25 N at a frequency of

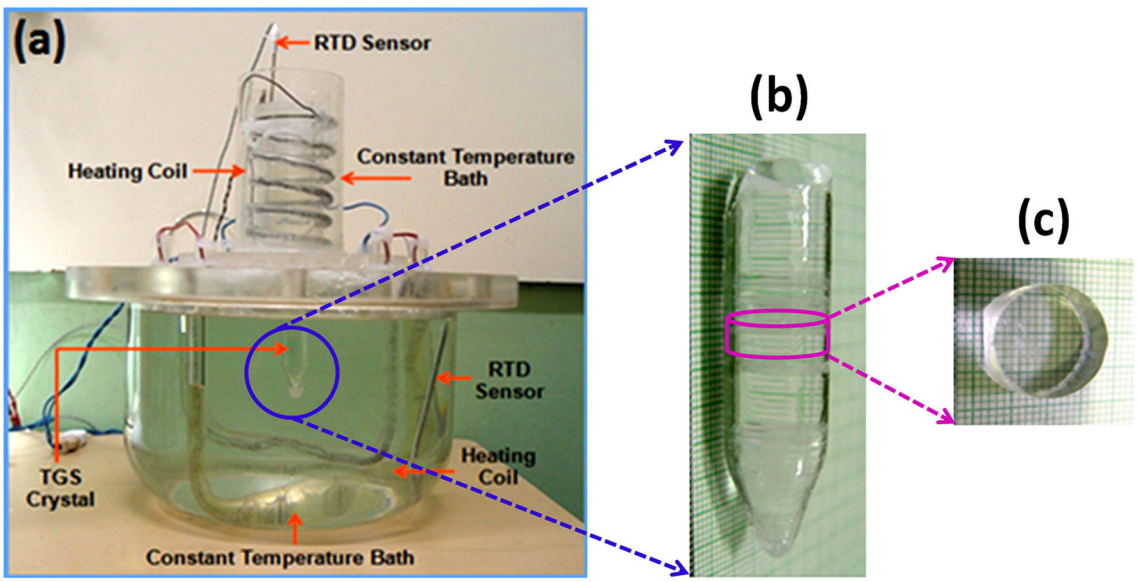

Fig. 1 **a** SR crystal growth apparatus used for TGS crystal growth below T_c. **b** [010]-oriented undoped TGS crystal grown below T_c, and **c** fabricated (010) device element

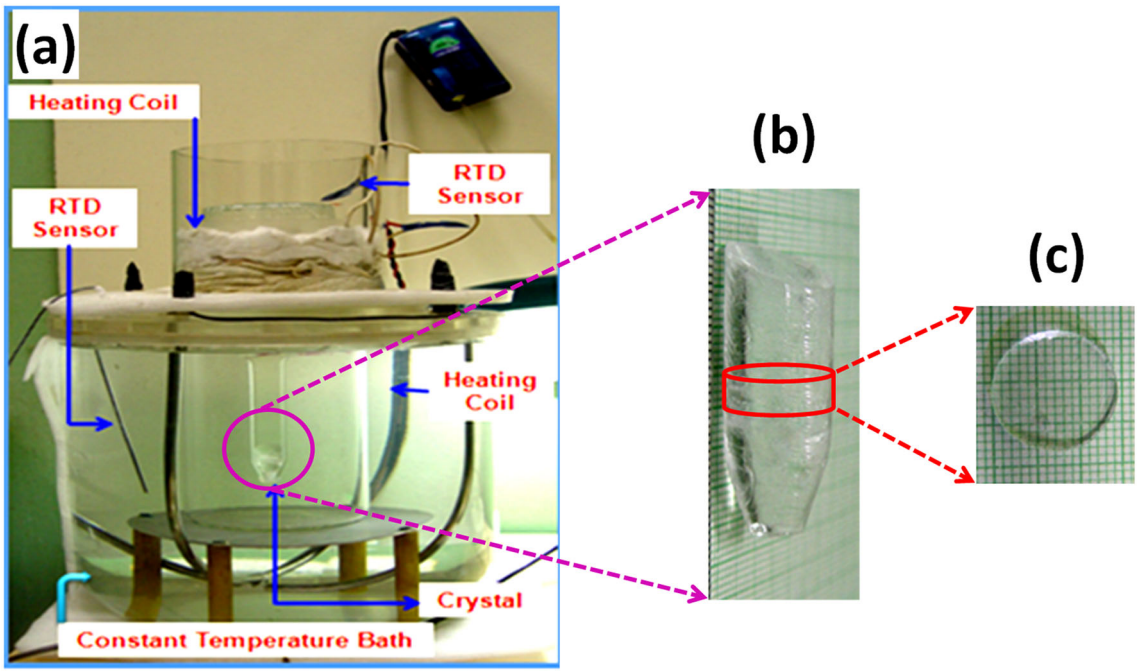

Fig. 2 **a** SR crystal growth apparatus used for TGS crystal growth above T_c. **b** [010]-oriented undoped TGS crystal grown above T_c, and **c** fabricated (010) device element

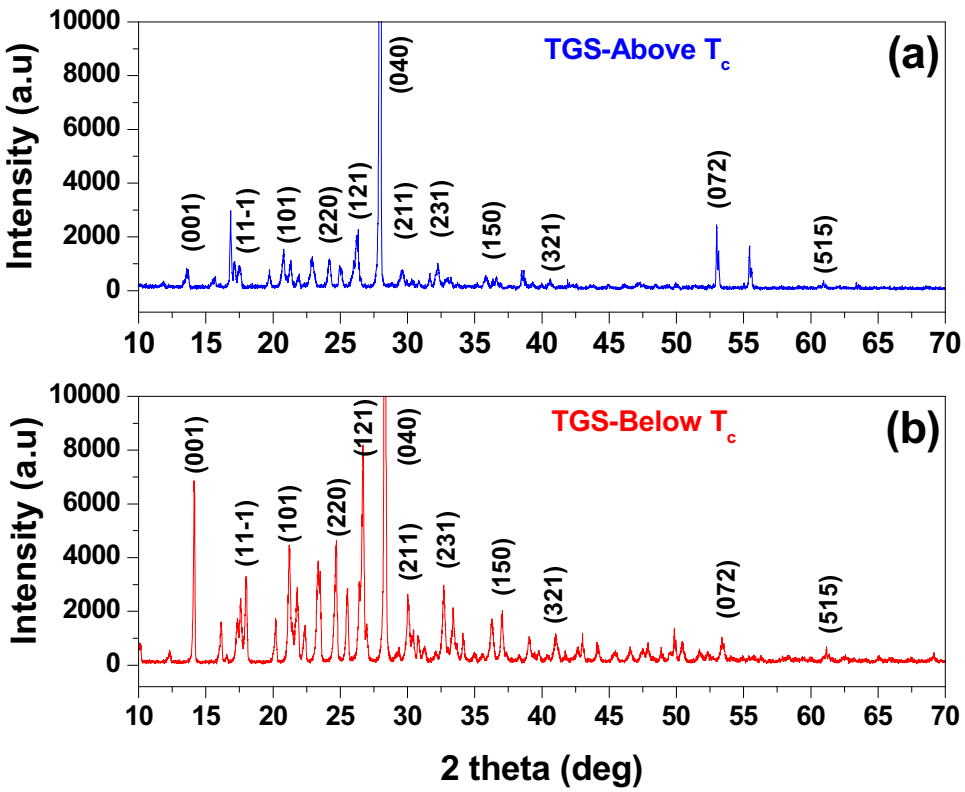

Fig. 3 Powder XRD patterns of the undoped TGS crystals grown **a** above and **b** below T_c

110 Hz that generated a charge on the TGS crystal under test. The d_{33} coefficient was measured directly in units of pC/N. The measured piezoelectric coefficient of TGS crystal grown below T_c was 45 pC/N,

and the value for the crystal grown above T_c was 16 pC/N. The higher value of d_{33} for crystal grown below T_c may be attributed to the higher concentration of point defects in this crystal as compared to the crystal grown above T_c, as the point defects favor the formation of ferroelectric domains. It is reported that high point defects cause slowing down of the domain wall movement and tend to reduce the piezoelectric coefficient [31]. In the case of TGS crystal grown above T_c, when the crystal is cooled to room temperature after growth, it makes the transition from paraelectric phase to ferroelectric phase, and in the process, a large number of domains nucleate in the ferroelectric phase, as has been reported by Costache et al. [32], which results in a decrease in domain mobility of above T_c grown crystal, and hence lower d_{33} coefficient.

2.3 *P–E* hysteresis loop analysis

P–E hysteresis loop measurements were performed on undoped TGS crystals grown below and above T_c with the help of the Sawyer–Tower circuit [33] using the Precision Work Station [Radiant Technology Inc.]. The crystal plates cleaved perpendicular to the polar b-axis from the bulk crystals were used for the purpose. The plates obtained in this way were polished using alumina powder as the polishing chemical, and ethylene glycol as the lubricant. Polished and highly transparent TGS sample plates of thickness 0.7 mm were chosen for the ferroelectric measurements. These sample plates were sputter-coated (Sputtering unit: EMITECH-K 550X model) with gold in the argon atmosphere on both sides to form electrodes. The maximum electric field applied for the P-E hysteresis measurements on the TGS crystal samples was ± 2.7 kV/cm. The relation between the remnant polarization (P_r), saturation polarization (P_s), and polarization at fields above the coercive field ($P_{1.1Ec}$) is given by [34].

$$R_{sq} = \frac{P_r}{P_s} + \frac{P_{1.1Ec}}{P_r}$$

where R_{sq} is the squareness of the hysteresis loop. Using this relation, the analysis of the *P–E* hysteresis loop of the samples of TGS crystals grown in ferroelectric and paraelectric temperature ranges was performed. The hysteresis loops observed on the oscilloscope, as shown in Fig. 4, are found to be symmetric in nature. The saturation value of the spontaneous polarization (P_s) for crystal grown below T_c was 0.48 μC/cm^2 and that for the crystal grown above T_c was 0.99 μC/cm^2. Also, Fig. 4 shows that the remnant polarization (P_r) of TGS grown above T_c was higher than that grown below T_c. The comparison of remnant polarization (P_r), saturation polarization (P_s), and coercive field (E_c) of undoped and differently doped TGS crystal grown by the present authors and those reported in the literature is presented in Table 1 [10, 35–37]. It has been reported in the literature that the dynamics of domain walls and their interaction with defects strongly influence the properties of the TGS crystal in the ferroelectric phase [38, 39]. The higher values of ferroelectric hysteresis parameters for crystal grown above T_c as compared to that grown below T_c may be attributed to higher point defects density in this crystal that influences the domain formation and hence influences the ferroelectric hysteresis properties more strongly as compared to the crystal grown below T_c.

2.4 Dielectric permittivity

The dielectric permittivity measurement of [010]-oriented undoped TGS crystals was carried out at different frequencies (100 Hz to 1 MHz) in the temperature range 25 to 65 °C during cooling. Crystal plates of size 6 × 6 × 1 mm^3 were coated with gold to make electrodes and thereafter subjected to dielectric measurements using an impedance analyzer (HP 4194 A Impedance / Gain phase analyzer). The cooling rate was maintained at 1 °C/min during

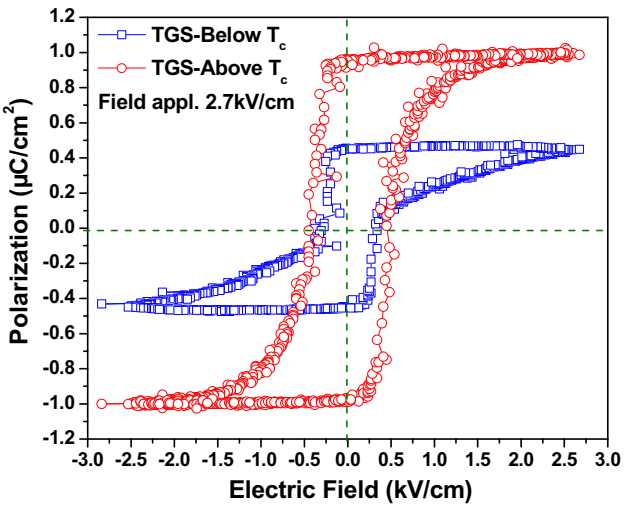

Fig. 4 Ferroelectric *P–E* hysteresis loops of the undoped TGS crystal grown below and above T_c

Table 1 Comparison of polarization versus electric field (*P*–*E*) data of the undoped and differently doped TGS crystals reported by the present authors and those reported in the literature by other researchers

TGS crystal	P_r (μC/cm^2)	P_s (μC/cm^2)	E_c (kV/cm)	− E_c (kV/cm)	References
Undoped TGS (below T_c)	0.44	0.48	0.34	− 0.26	Present work
Undoped TGS (above T_c)	0.94	0.99	0.50	− 0.45	
Urea-TGS (below T_c)	0.60	0.62	1.5	− 0.5	[10]
Urea-TGS (above T_c)	0.003	Unsaturated *P*–*E* values			
Undoped TGS (below T_c)	1.19	–	1.7	− 1.4	[35]
Undoped TGS (below T_c)	1.01	1.10	1.61	− 1.2	[36]
Maleic acid doped TGS (below T_c)	1.27	1.34	1.24	− 1.1	
Undoped TGS (below T_c)	2.5	2.7	0.88	− 0.88	[37]
1 mol% IDA doped TGS (below T_c)	1.7	1.9	1.62	− 1.2	
5 mol% IDA doped TGS (below T_c)	1.8	2.1	4.2	− 1.8	
10 mol% IDA doped TGS (below T_c)	3.1	3.3	2.1	− 5.9	

measurements. Figure 5a, b shows the temperature dependence of the dielectric constant for TGS crystals (grown above and below T_c) at a probing frequency of 100 kHz. It is clear from Fig. 5 that dielectric constant (ε) increases anomalously in the vicinity of phase transition temperature, i.e., near 49 °C. The crystal grown above T_c shows a higher value of maximum dielectric constant as compared to the crystal grown below T_c. The dielectric constants of the crystal grown above and below T_c are 14,386 and 13,092, respectively. Another important feature of Fig. 5 is the presence of a step-like increase in dielectric constant and associated asymmetric fall in its values for the crystal grown above T_c. This feature is typical of archetypical ferroelectric single crystal such as $BaTiO_3$ with the emergence of spontaneous polarization at the phase transition temperature. For the crystal grown below T_c, the step-like rise in dielectric constant (during cooling) is comparatively diffuse. The observed behavior of the dielectric constant may be attributed to the difference in the interaction between point defects and domain walls in the TGS crystals grown below and above T_c. In TGS crystal grown above T_c, the defects are randomly distributed. Therefore, the domain walls are not surrounded by point defects, resulting in their higher mobility. This manifests in higher ε_r for TGS crystal grown above T_c as compare to that grown below T_c. Further, the symmetric nature of the dielectric constant curve for TGS crystal grown below T_c

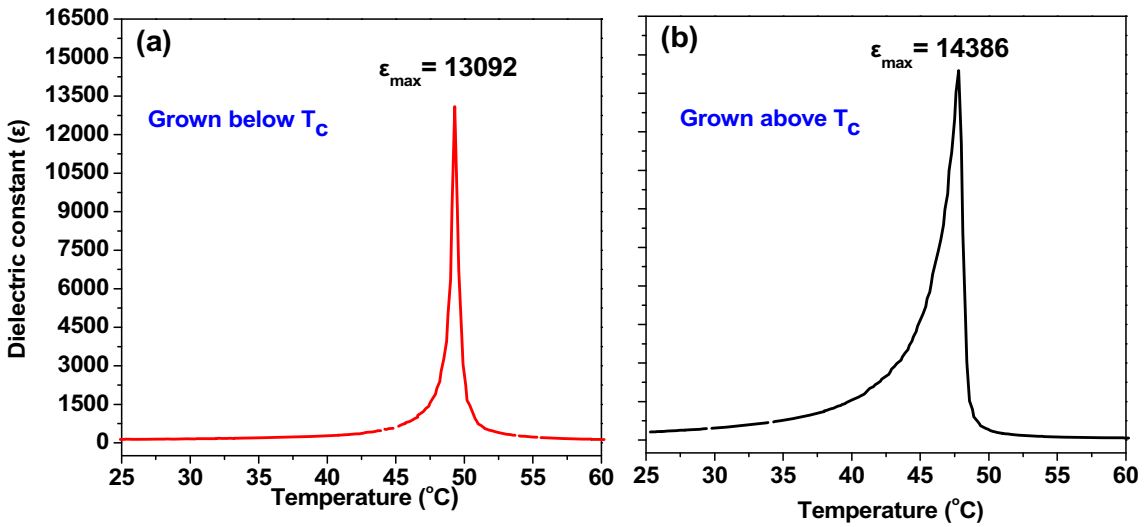

Fig. 5 Variation of dielectric permittivity at different temperatures at frequency of 100 kHz for the undoped TGS crystal grown **a** below T_c and **b** above T_c

represents the situation when the domain walls are surrounded by a cloud of point defects leading to blocking of domain wall movement. On the other hand, in the case of crystal grown above T_c, a redistribution of point defects takes place because of thermal effects. As a result, the defects are distributed randomly throughout the bulk of the crystal instead of being concentrated near the domain wall.

2.5 Dislocation defects characterization

The chemical etching was performed for quantifying dislocation defects in TGS crystals grown below and above T_c. Water was used as the etchant, and the etched crystal surface was imaged under an optical microscope (Olympus U-TV0.5XC-3, Japan). Figure 6a and b shows the etch pit patterns after etching for 5 s, as formed on the (010) face of TGS crystal grown below T_c (ferroelectric phase temperature range) and that grown above T_c (paraelectric phase temperature range). In both, the etch pits are randomly distributed, oval in shape, and oriented parallel to each other. The etch pit density (EPD) was calculated using the formula:

$$\text{Etch pit density (EPD)} = \frac{\text{number of etch pits in the area imaged}}{\text{area}}.$$

The crystal surface area imaged under the microscope was $200 \times 150\ \mu m^2 = 3 \times 10^{-4}\ cm^2$. The number of etch pits that appeared in this given area was 45 and 20 for below and above T_c grown TGS crystal, respectively. Therefore, the etch pit density (EPD) for below and above T_c was 1.5×10^5 dislocations/cm^2 and 6.67×10^4 dislocations/cm^2, respectively. The different dislocation densities could be attributed to the following reasons [40–42]: (1) The quality of the seed crystal with respect to the defects structure, especially the dislocation density, (2) growth process conditions, such as temperature and cooling rates, and (3) the post-growth crystal processing conditions, such as cutting, lapping and polishing procedure. Since the third step was identical in the two crystal growth experiments, therefore the lower etch pit density of the crystal grown above T_c could be attributed to the first two parameters, namely the quality of the seed crystal and the different growth conditions. No other defects such as solvent inclusions, growth striations, and low angle grain boundaries are observed in the bulk TGS crystals grown below and above T_c.

2.6 Vickers microhardness

The mechanical properties of the grown TGS crystals are of vital importance in fabricating device elements such as that required in IR detectors [39]. Vickers microhardness is a measure of mechanical strength of a material calculated from the size of an impression produced under load by a pyramid-shaped diamond indenter. The microhardness studies were carried out on (010) plates of TGS crystals grown below and above T_c using an automatic digital microhardness tester fitted with a Vickers diamond pyramid indenter (Matsuzawa MMTX-7, Japan) with loads of 10, 25, 50, 100, and 200 g at room temperature. TGS crystal plates of 2 mm thickness were cut and polished from the as-grown crystal for these measurements. The indentation time was 5 s for all the loads, and the microhardness value was taken as the average of

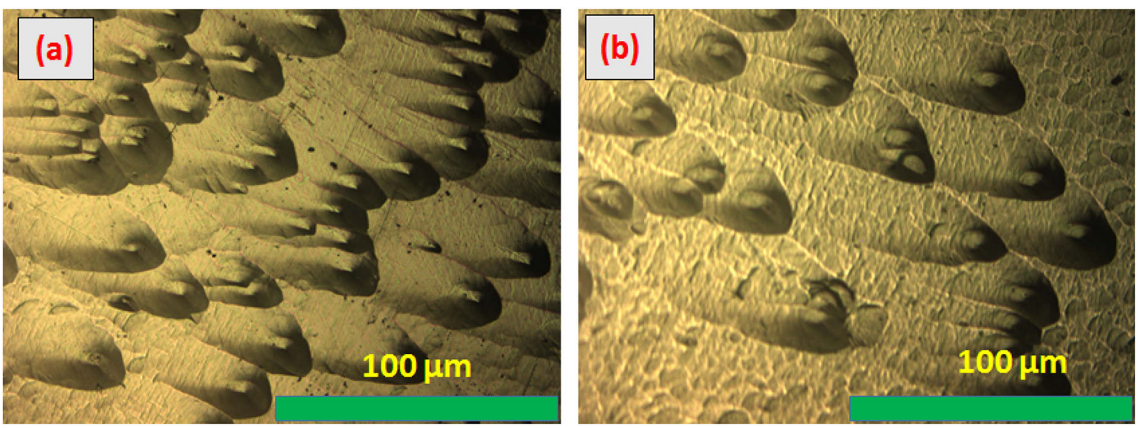

Fig. 6 Etch pit patterns on (010) habit faces of the undoped TGS crystals grown **a** below and **b** above T_c

several impressions made with the same load. The hardness number (H_v) was calculated using the relation:

$$H_v = \frac{(1.854\,P)}{d^2}\ \mathrm{kg/mm^2}.$$

where H_v is the Vickers hardness number (kg/mm^2), P is the applied load (g) and d is the average diagonal length (mm) of the indentation mark. In the case of TGS crystal grown below T_c, a rise in hardness number was observed up to 100 g, when the maximum hardness of 98.5 kg/mm^2 was obtained. Above 100 g load, micro-cracks were observed on the crystal plate. For TGS crystal grown above T_c, the microhardness shows a steep increase with the increase in the applied load up to 200 g load, where a maximum hardness of 263.2 kg/mm^2 was obtained. Above 200 g of load, the cracks were developed around the indentation mark. The values of microhardness as a function of the applied load are shown in Fig. 7 for both the crystal samples. The three-times increase in hardness values for above T_c grown crystals makes them more suitable for devices using (010) plates. An increase in the hardness will lead to an improvement in device element fabrication and processing due to lesser cracks/breakage during mechanical processing. The indentation impressions on (010) plates of TGS crystals grown below and above T_c by the Vickers microhardness tester under 100 g load are shown in Fig. 8a, b, respectively. The figure shows cracks originating from the corners of the indentation, which are higher in the case of crystal grown above T_c as compared to that grown below T_c. At loads lower than 100 g, such impression appears to be free of cracks, but for loads greater than 100 g the micro-cracks are well defined. The hardness depends on the applied indentation (load P), the crystallographic face and the bonds in the material in that crystallographic orientation. In addition, it is reported in the literature on mechanical properties of the crystals, the hardness of the crystals is intricately linked to the concentration of point defects. The higher the concentration of point defects in a crystal, the higher is its microhardness [43, 44]. Since the hardness of TGS grown above T_c is more than that of TGS grown below T_c, therefore this may be attributed to the higher point defects in the above T_c grown crystal. This result is consistent with the behavior of piezoelectric coefficient and P–E hysteresis studies,

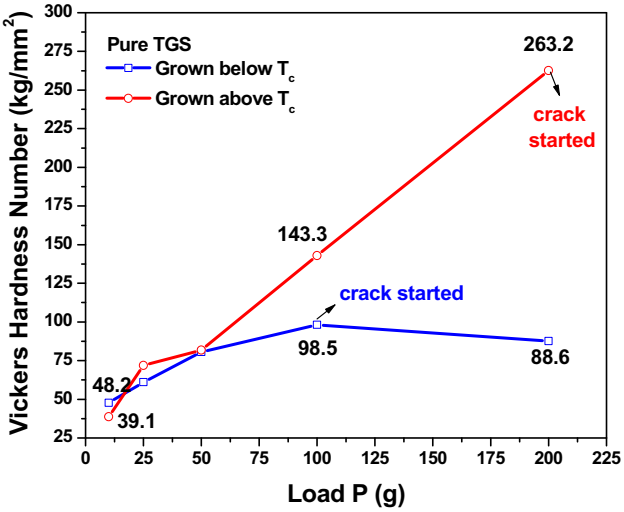

Fig. 7 Vickers microhardness versus load for the undoped TGS crystals grown below and above T_c grown

which were also explained on the basis of point defects in these crystals.

2.7 UV–Vis NIR transmission

The optical quality of the TGS crystals grown below and above T_c was measured by spectrophotometer (JASCO V-670) in the wavelength range 190 nm to 2200 nm. TGS crystals were sliced by a diamond cutter to get a plate of 2 mm thickness, which was subsequently smoothened and polished to obtain sample plates of 1 mm thickness. Figure 9 shows the transmission of nearly 83% for the 1 mm thickness of undoped TGS crystal grown below T_c and the transmission of 79 % for the sample of identical thickness from the crystal grown above T_c. Defects such as inclusions, bubbles, precipitates are detrimental to the crystal quality as these result in absorption, scattering, and refractive index variations. The crystals samples used for transmittance measurements were free from any of these defects, resulting in high transmittance of both the sample.

Table 2 summarizes various device-relevant properties of [010]-oriented undoped TGS crystals grown above and below Curie temperature by unidirectional solution growth SR method. All the measurements reported in Sects. 3.1 to 3.7 were performed under identical sample conditions such as thickness and surface polish.

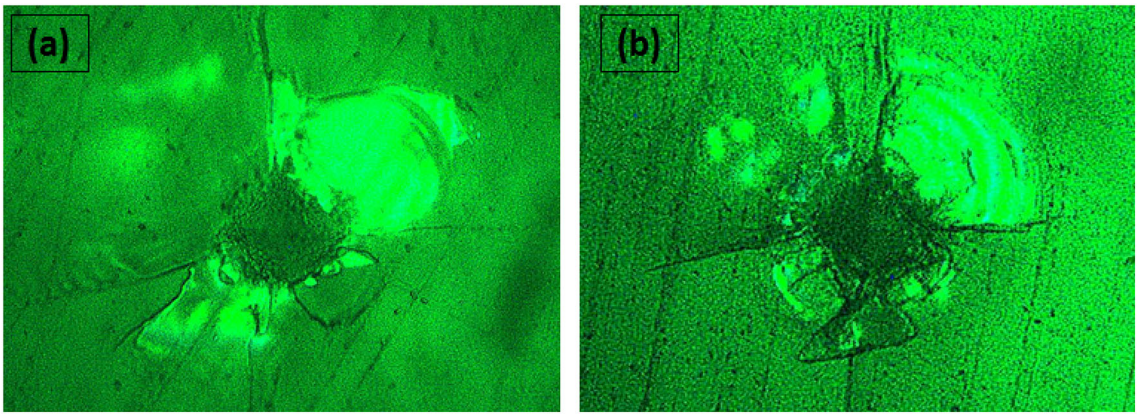

Fig. 8 Indentation pattern and micro-cracks at the corners, under 100 g load for the undoped TGS crystal grown **a** below and **b** above T_c

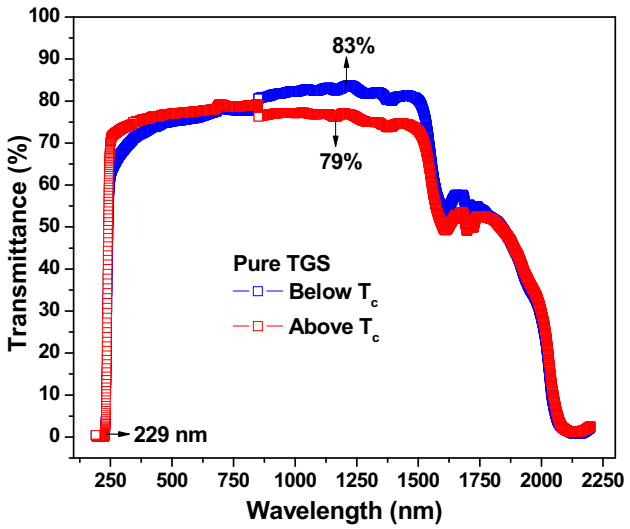

Fig. 9 UV–Vis NIR spectrum of the undoped TGS crystals grown below and above T_c

3 Conclusions

Undoped ferroelectric single crystals of TGS grown by unidirectional solution growth method along [010] polar direction in temperature ranges above and below T_c were characterized for important figures of merit such as phase analysis, piezoelectric coefficient, ferroelectric *P–E* hysteresis loop, dielectric permittivity, defects density, mechanical hardness, and optical quality. The powder XRD pattern of the two crystals shows diffraction peaks appearing at the same diffraction angle position. The variation in the intensity of the peaks is attributed to the difference in defects structure, especially point defects in the TGS crystals grown below and above T_c. The difference in piezoelectric behavior of the two crystals is explained based on the difference in the points defects concentration and their influence on the mobility of domain walls in the two crystals, with a higher piezoelectric coefficient for the crystal grown below T_c. *P–E* hysteresis studies for TGS crystals grown

Table 2 Summary of the device-relevant properties of [010]-oriented undoped TGS crystals grown above and below Curie temperature by unidirectional solution growth SR method

Crystal property	TGS crystal grown below T_c	TGS crystal grown above T_c
Piezoelectric coefficient	45 pC/N	16 pC/N
Ferroelectric *P–E* hysteresis values	P_r = 0.44 μC/cm^2	P_r = 0.94 μC/cm^2
	P_s = 0.48 μC/cm^2	P_s = 0.99 μC/cm^2
	E_c = 0.34 kV/cm	E_c = 0.50 kV/cm
	− E_c = 0.26 kV/cm	− E_c = 0.45 kV/cm
Dielectric permittivity at 49 °C	13,092	14,386
Dislocation density (measured by finding the etch pit density (EPD))	1.5 × 10^5 dislocations/cm^2	6.67 × 10^4 dislocations/cm^2
Maximum Vickers microhardness	98.5 kg/mm^2 at 100 g	263.2 kg/mm^2 at 200 g
Transmittance in NIR region	83%	79%

above as well as below T_c show well-saturated symmetrical hysteresis loops, with higher values of remnant polarization (0.94 μC/cm^2) and coercive field (0.50 kV/cm) for crystal grown above T_c as compared to those for TGS grown below T_c (0.44 μC/cm^2 and 0.34 kV/cm). The variation in the dielectric permittivity (ε_r) of the TGS crystal grown below T_c and above T_c is attributed to the difference in the defects structure of the two crystals. The Vickers microhardness measurement shows that the crystals grown above T_c have higher H_v values than those grown below T_c. The two crystal samples show minor variations in the density of dislocations and the optical transmittance. Based on piezoelectric studies, ferroelectric *P–E* hysteresis loop analysis, dielectric results, dislocation density, and microhardness characterization results, it is concluded that undoped TGS crystal grown above T_c has improved physical properties as compared to that grown below T_c.

Acknowledgements

M. Senthil Pandian is grateful to RRCAT authorities for granting six months project internship and extending various characterization facilities. Late Prof. R. Gopalakrishnan, Anna University, is acknowledged for the microhardness measurements.

References

1. B.T. Matthias, C.E. Miller, J.P. Remeika, Phys. Rev. **104**, 849–850 (1956)
2. G. Arunmozhi, E. De Matos Gomes, J.L. Ribeiro, Ferroelectrics **295**, 87–95 (2003)
3. H.P. Beerman, Ferroelectrics **2**, 123–128 (1971)
4. A.K. Batra, P. Guggilla, D. Cunningham, M.D. Aggarwal, R.B. Lal, Phys. B **371**, 210–214 (2006)
5. X. Sun, M. Wang, Q.W. Pan, W. Shi, C.S. Fang, Cryst. Res. Technol. **34**, 1251–1254 (1999)
6. J.M. Chang, A.K. Batra, R.B. Lal, J. Cryst. Growth **158**, 284–288 (1996)
7. H.H. Wieder, C.R. Parkerson, J. Phys. Chem. Solids **25**, 241–245 (1964)
8. N. Nakatani, M. Yoshio, Jpn. J. App. Phys. **35**, L508–L510 (1990)
9. P.J. Lock, Appl. Phys. Lett. **19**, 390–391 (1971)
10. M. Senthil Pandian, S. Verma, P. Ramasamy, G. Singh, S.M. Gupta, V.S. Tiwari, A.K. Karnal, Appl. Phys. A **126**, 492 (2020)
11. M. Senthil Pandian, S. Verma, P. Karuppasamy, V. Padmanabhan, P. Ramasamy, V.S. Tiwari, A.K. Karnal, J. Cryst. Growth **546**, 125793 (2020)
12. M. Senthil Pandian, S. Verma, P. Karuppasamy, P. Ramasamy, V.S. Tiwari, A.K. Karnal, Mater. Res. Bull. **134**, 1–9 (2021)
13. N. Sinha, N. Goel, B.K. Singh, M.K. Gupta, B. Kumar, J. Solid State Chem. **190**, 180–185 (2012)
14. O.V. Rogazinskaya, S.D. Milovidova, A.S. Sidorkin, O.B. Yatsenko, A.N. Yuryev, Z.D. Stekhanova, Ferroelectrics **307**, 251–254 (2004)
15. R.B. Lal, A.K. Batra, J.D. Trolinger, W.R. Wilcox, Microgravity Q **4**, 186–198 (1994)
16. S. Ballard, K. Mccarthy, Phys. Rev. **90**, 375–378 (1953)
17. T. Krajewski, F. Jaroszyk, Acta Phys. Pol. A **43**, 831–843 (1973)
18. E.T. Keve, K.L. Bye, P.W. Whipps, A.D. Anis, Ferroelectrics **3**, 39–48 (1971)
19. I. Shibuya, T. Mitsui, J. Phys. Soc. Japan **16**, 479–489 (1961)
20. J.A. Gonzalo, Phys. Rev. **144**, 662–665 (1966)
21. M. Koralewski, B. Jimenez, J. De Frutos, B. Noheda, J.A. Gonzalo, Ferroelectrics **157**, 263–268 (1994)
22. I.S. Girnyk, O.S. Kushnir, R.Y. Shopa, Ferroelectrics **317**, 75–78 (2005)
23. B. Andriyevsky, W. Ciepluch Trojanek, A. Patryn, Conden. Matt. Phys. **10**, 33–38 (2007)
24. K. Biedrzycki, Ferroelectrics **192**, 269–277 (1997)
25. N. Sinha, S. Bhandari, H. Yadav, G. Ray, S. Godara, N. Tyagi, J. Dalal, S. Kumar, B. Kumar, CrystEngComm **17**, 5757–5767 (2015)
26. E.A.D. White, J.D.C. Wood, V.M. Wood, J. Cryst. Growth **32**, 149–156 (1976)
27. S. Dinakaran, S. Verma, S. Jerome Das, S. Kar, K.S. Bartwal, P.K. Gupta, Phys. B **405**, 1809–1812 (2010)
28. P. Karuppasamy, T. Kamalesh, M. Senthil Pandian, P. Ramasamy, S. Verma, J. Crystal Growth **518**, 59–72 (2019)
29. V. Govindan, D.J. Daniel, P.Q. Vuong, K. Sankaranarayanan, H.J. Kim, J. Cryst. Growth **531**, 125344 (2020)
30. S.K. Kushwaha, N. Vijayan, G. Bhagavannarayana, Mater. Lett. **62**, 3931–3933 (2008)
31. X. Guisheng, L. Haosu, W. Pingchu, X. Haiqing, Y. Zhiwen, Chin. Sci. Bull. **45**, 491 (2000)
32. M. Costache, I. Matei, L. Pintilie, H.V. Alexandru, C. Berbecaru, J. Optoelectronics Adv. Mater. **3**, 75 (2001)
33. C.B. Sawyer, C.H. Tower, Phys. Rev. **35**, 269–273 (1930)
34. J. Novonty, J. Zelinka, Z. Podvalova, Ferroelectrics **313**, 1–6 (2004)

35. M. Senthil Pandian, P. Ramasamy, B. Kumar, Mater. Res. Bull. **47**, 1587–1597 (2012)
36. A. Hussain, N. Sinha, A.J. Joseph, S. Goel, B. Singh, I. Bdikin, B. Kumar. Arab. J. Chem. **13**, 1874–1889 (2020)
37. B. Chitharanjan Rai, S.M. Narayana Moolya, Dharmaprakash, Phys. B **406**, 1–7 (2011)
38. S.A. Gridnev, V.V. Gorbatenko, B.M. Prasolov, Ferroelectrics **164**, 349–352 (1995)
39. S.A. Gridnev, L.A. Safonova, A.V. Biryukov, A.N. Tsotsorin, Ferroelectrics **234**, 139–146 (1999)
40. S. Amelinckx, *Direct Observation of Dislocations* (Academic Press, Cambridge, 1964), p. 21
41. K. Sangwal, *Etching of Crystals, Theory, Experiments and Applications* (North Holland, Amsterdam, 1987).
42. K. Li, P. Yang, D. Xue, Acta Mater. **60**, 35–42 (2012)
43. D. Hull, *Introduction to Dislocations*, 2nd edn. (Pergamon Press, Oxford, 1975).
44. A.A. Urusovskaya, Chap. 2: Mechanical Properties of Crystals, in *Modern Crystallography IV: Physical Properties of Crystals*, ed. by L.A. Shuvalov (Springer, Berlin, 1988), pp. 50–177